Global sensitivity analysis of offshore wind turbine foundation fatigue loads

Velarde, Joey; Kramhøft, Claus; Sørensen, John Dalsgaard

Published in:
Renewable Energy

DOI (link to publication from Publisher):
10.1016/j.renene.2019.03.055

Publication date:
2019

Document Version
Publisher's PDF, also known as Version of record

Renewable Energy 140 (2019) 177–189

Contents lists available at ScienceDirect

Renewable Energy

journal homepage: www.elsevier.com/locate/renene

Global sensitivity analysis of offshore wind turbine foundation fatigue loads

Joey Velarde [a, b, *], Claus Kramhøft [a], John Dalsgaard Sørensen [b]

[a] Marine and Foundation Engineering, COWI A/S, 8000 Aarhus, Denmark
[b] Department of Civil Engineering, Aalborg University, 9220 Aalborg, Denmark

ARTICLE INFO

Article history:
Received 20 April 2018
Received in revised form
22 December 2018
Accepted 11 March 2019
Available online 15 March 2019

Keywords:
Offshore wind turbine
Gravity based foundation
Fatigue
Sensitivity analysis
Monte Carlo
Morris screening

ABSTRACT

The design and analysis of offshore wind turbine foundations are traditionally based on deterministic time-domain simulations of a numerical model. The wind turbine, support structure and environmental conditions are represented by a large number of input parameters, whose uncertainties are accounted by applying partial safety factors. In this paper, the sensitivity of fatigue loads with respect to primary structural, geotechnical and metocean parameters are investigated for a 5 MW offshore wind turbine installed on a gravity based foundation. Linear regression of Monte Carlo simulations and Morris screening are performed for three design load cases. Results show that parameter significance rankings vary according to which design load case is considered. In general, uncertainties in the fatigue loads are highly influenced by turbulence intensity and wave load uncertainties, while uncertainties in soil property suggest significant nonlinear or interactive effects. This work provides insights to foundation designers and wind turbine manufacturers on which parameters must be assessed in more detail in order to reduce uncertainties in load prediction.

1. Introduction

The design of offshore wind turbine (OWT) support structures requires evaluations against a number of design load cases (DLC's) as outlined in several design standards [1–3]. Ideally, limit state analyses are performed using integrated structural models to capture the complex interactions between the OWT structure and the environment, as illustrated in Fig. 1. Despite uncertainties related to parameter estimation and numerical representation of wind, wave, soil and structure, deterministic approaches are normally performed, where partial safety factors are used to account for load and resistance uncertainties. Probabilistic design approaches, on the other hand, allow more rigorous consideration of parameter uncertainties, particularly site-specific environmental inputs, at the expense of higher calculation times. In this regard, identification of the most significant sources of uncertainties, i.e. by performing a global sensitivity analysis of a fully coupled aero-hydro-servo-elastic model, becomes important.

Sensitivity analysis (SA) refers to the study of how uncertainty in the model output can be decomposed into different sources of uncertainties in the model input [4]. Derivative-based approaches, where parameter sensitivity is measured in terms of the change in model output with respect to an incremental change in the input, are most common in literature due to its efficiency. However, for nonlinear models involving a high number of uncertain parameters, the sensitivity measured at a particular reference point may not be valid throughout the whole input space. Global SA approaches, on the other hand, consider different points across the input space to obtain a more representative variation in the output [4]. Some examples of global SA techniques include linear regression of Monte Carlo simulations [5], Morris screening [6], and variance-based methods [4].

Sensitivity analyses and probabilistic design approaches have been applied in the field of OWT support structure design, where most studies distinguish analysis between different sources of uncertainties. The effect of accounting for geotechnical uncertainties [7,8], mostly due to inherent soil spatial variability, were investigated by several researchers [9–13]. Results show that stochastic soil properties has a huge influence on OWT dynamic responses, and thus affect reliability estimates. For hydrodynamic loads, a general source of uncertainty is the choice of wave load model. A review of numerical simulation tools for offshore wind

* Corresponding author. Marine and Foundation Engineering, COWI A/S, 8000 Aarhus, Denmark.
E-mail address: jovl@cowi.com (J. Velarde).

https://doi.org/10.1016/j.renene.2019.03.055

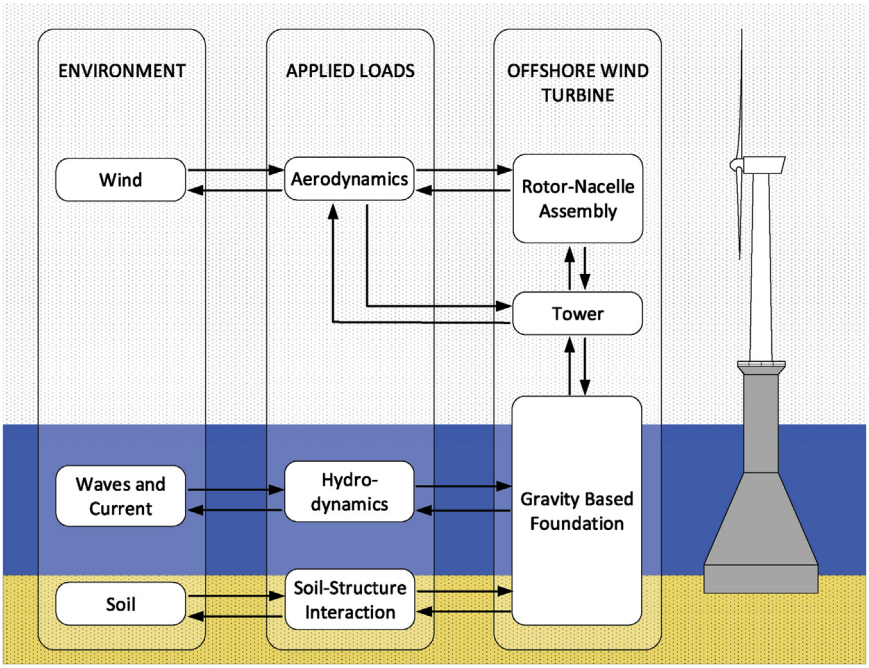

Fig. 1. Interaction between wind loads, wave loads, soil and an offshore wind turbine.

turbines by Vorpahl et al. [14] outlines the differences in wave modeling approaches. The validation of these numerical tools performed under the OC5 Project [15] also showed significant differences in load predictions, particularly at shallow water depths where the effect of wave nonlinearities become more important. A sensitivity analysis of offshore monopile fatigue loads accounting for wave and soil parameter variations was performed by Glišić et al. [16]. Using 1st order Sobol indices, results showed that wave load parameters highly influence the stresses. With regards to wind climate parameters, most sensitivity analyses were performed for onshore wind turbines. Toft et al. [17,18] showed that wind parameter uncertainties account for about 10–30% of uncertainties in structural reliability of wind turbine components, and that fatigue loads are most sensitive to variation in turbulence intensity. Murcia et al. [19] demonstrated the use of polynomial response surfaces in fatigue analysis. Using Sobol variance decomposition, turbulence intensity was also found to be a significant parameter for fatigue.

A notable global SA was performed by Hübler et al. [20], where a multi-step approach was applied to a monopile and a jacket foundation considering soil, wind, wave and structural uncertainties. Results showed that only a few parameters are influential and other inputs can be treated deterministically without losing accuracy. While most of the above-mentioned studies were based on crude Monte Carlo simulations, other methods for global SA, particularly Morris screening, has also been demostrated by Martin et al. [21] in offshore wind farm operations and maintenance [21] and by Ziegler & Muskulus [22] in fatigue reassessment for lifetime extension of monopile substructures.

In this paper, linear regression of Monte Carlo simulations and Morris screening were applied to investigate the sensitivity of OWT support structure fatigue loads with respect to primary structural and environmental parameters. Dynamic simulations of a 5 MW OWT supported by a gravity based foundation (GBF) were performed in HAWC2 [23]. To investigate the dependence of parameter significance with the design load case (DLCs) considered, the analyses were performed for three different DLCs: fatigue limit state (FLS) analysis during power production, FLS analysis during parked or idling conditions, and an extreme case with wind speed above the WT cut-out wind speed. An example with the two global SA methods is performed to verify the sensitivity analysis and the resulting parameter significance rankings.

2. Methods

This section describes the general procedure for structural modeling and fatigue simulation of an offshore wind turbine supported by a concrete GBF. The selected variable inputs related to structural properties, soil parameters, and metocean conditions are also presented. The two sensitivity analyses methods employed, the Monte Carlo (MC) and Morris Screening (MS) methods, are also discussed.

2.1. Wind turbine modeling

The selected reference project is the GBF concept adopted at the Thornton Bank offshore wind farm (Phase 1), which was installed in the Belgian North Sea (LAT 51.55°, $LONG$ 2.92°) about 35 km off the coast of Ostend. The wind farm has a total capacity of 30 MW from six - 5 MW REpower offshore wind turbines. Among the six GBFs, the foundation exhibiting both the softest soil condition and the highest average water depth was chosen for detailed structural modeling.

Several research and commercial aero-servo-hydro-elastic codes are available to model and simulate time-domain structural response of an offshore wind turbine. The simulation tool *HAWC2 (Horizontal Axis Wind turbine simulation Code 2nd generation)* [23] developed by Technical University of Denmark (DTU) - Risø was used to develop a fully-coupled GBF model.

2.1.1. Support structure and wind turbine model

The structural analysis in HAWC2 code follows a multibody formulation, where each body consists of Timoshenko beam elements [23] with 6 degrees of freedom (x). For a defined mass matrix

[M], damping matrix [D] and stiffness matrix [K], the general equation of equation with aerodynamic (F_{aero}) and hydrodynamic (F_{hydro}) forces can be expressed as:

$$[M]\ddot{x} + [D]\dot{x} + [K]x = F_{aero} + F_{hydro} \quad (1)$$

The Thornton Bank GBF is modeled in HAWC2 as shown in Fig. 2. The GBF has a conical shape with a base diameter of 23.5 *m*, which is constantly tapered to 6.5 *m* at the lower ring beam. The interface, located at 14.7 *m AMSL*, connects the upper ring beam and the steel tower with $OD = 5.5\ m$. Both concrete GBF and steel tower are modeled as axis-symmetric sections having linearly elastic material characterized by mean Young's modulus ($E_s = 210\ GPa$, $E_c = 29.6\ GPa$) and structural shear modulus ($G_s = 80.8\ GPa$, $G_c = 15.0\ GPa$). The wind turbine, including the blade structural and aerodynamic properties, are based on the NREL 5 MW reference wind turbine [24], which was developed with similar properties as the REpower 5 MW wind turbine. The mean water depth and hub height are 25 *m* and 91.7 *m AMSL*, respectively.

The overall damping (D_{total}) of an offshore wind turbine can be estimated from the linear combination of aerodynamic (D_{aero}), hydrodynamic (D_{hydro}), structural (D_{struc}) and foundation damping (D_{soil}) [25,26]. In addition, contributions from mass dampers (D_{damper}), if any, should be included. Equation (2) shows the damping contributions considered in this study.

$$D_{total} = D_{aero} + D_{hydro} + D_{struc} + D_{soil} \quad (2)$$

In HAWC2, both aerodynamic and hydrodynamic contributions are calculated as a function of the environmental inputs (i.e. wind speed, water depth, wind and water densities). The rest of the components can be accounted by defining the damping coefficients, which can be done for each structural "bodies" that make up the whole offshore wind turbine. HAWC2 implements a Rayleigh viscous damping formulation [27], where the damping matrix is expressed as a linear combination of both mass and stiffness matrices as shown in Equation (3). The constants α and β are the mass and stiffness-proportional coefficients, respectively. For simplicity, only stiffness-proportional damping is considered, and both foundation and structural damping contributions are implemented at the tower multibody. The β is tuned to achieve a combined soil D_{soil} and structural D_{struc} damping of 1.10 % for the first fore-aft mode, which is a typical assumption in practice and has been verified by several offshore measurement campaigns [26,28]. A free vibration analysis shown in Fig. 3 was conducted in HAWC2 to validate the damping formulation. For underdamped systems under free vibration, the ratio of two successive amplitudes can be described by the logarithmic decrement (δ) defined in Equation (4). Consequently, the damping ratio (ζ) can be calculated from Equation (5).

$$D_{struc} + D_{soil} = \alpha M + \beta K \quad (3)$$

$$\delta = ln\frac{A_1}{A_2} \quad (4)$$

$$\zeta = \frac{\delta}{\sqrt{(2\pi)^2 + \delta^2}} \quad (5)$$

For GBFs, the dynamic foundation stiffness can be determined using recommendations from the design standard for offshore wind turbines by DNV [3]. Based on elastic theory, the lateral K_H and rotational K_R stiffness values can be calculated using Eq. (6) and

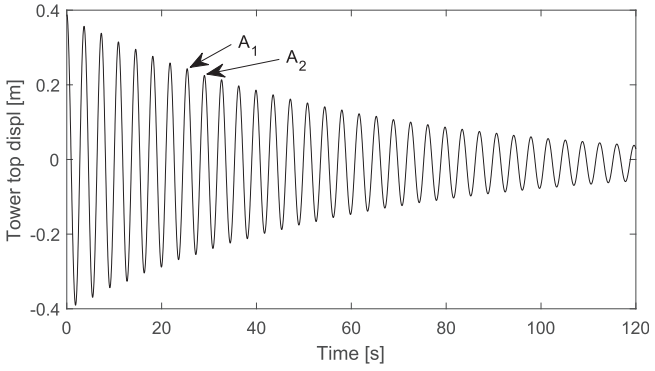

Fig. 3. Free vibration test with initial tower top displacement of 0.40 *m*.

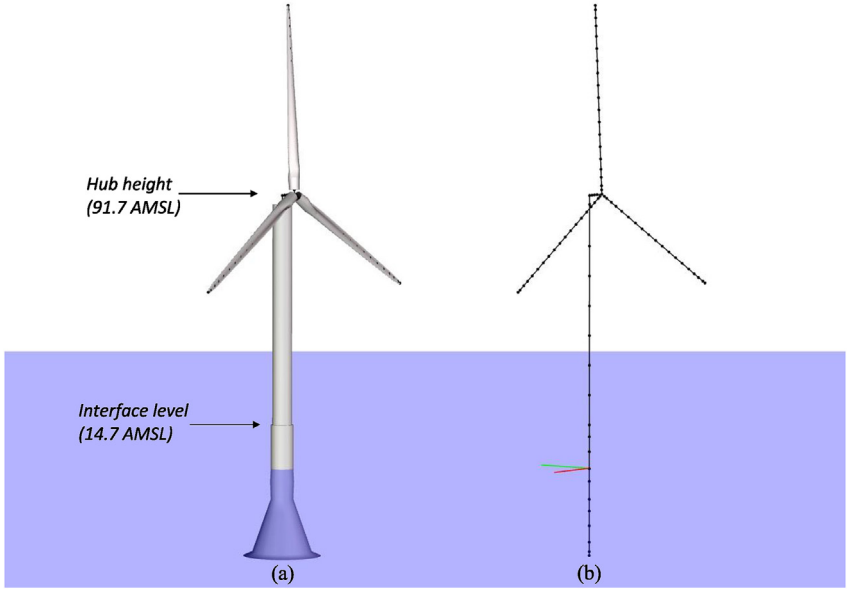

Fig. 2. GBF model visualization in HAWC2: (a) surface model, (b) beam elements.

Eq. (7). The parameters G, ν, and H refer to soil dynamic shear modulus, Poisson's ratio and height of soil strata, respectively. For wind turbines under moderate environmental conditions, it is assumed that no significant soil deformation occurs, such that soil reactions can be represented using linear elastic theory. Furthermore, it is assumed that the soil layers are fairly homogeneous. The foundation is represented in HAWC2 using the apparent fixity (AF) approach [29], where an equivalent beam element fixed at a determined distance below the foundation base is used to represent the soil stiffness (K_H, K_R). The equivalent length (L) is determined based on elementary beam theory and mudline loads during operation.

$$K_H = \frac{8GR}{2-\nu}\left(1+\frac{R}{2H}\right) \tag{6}$$

$$K_R = \frac{8GR^3}{3(1-\nu)}\left(1+\frac{R}{6H}\right) \tag{7}$$

The OWT model is a multi-degree of freedom (MDOF) system with several eigenfrequencies and mode shapes. The damped or undamped eigenvalue analysis of the total system can be performed in HAWC2 [23] including all constraint equations. The damped natural frequency is chosen as the output, to assess the relative importance of the combined soil and structural damping.

2.1.2. Environmental load cases

A number of design load cases (DLCs) has to be evaluated for certification of offshore wind turbine structures. Among the DLCs outlined in the IEC (International Electrotechnical Commission) standards [1,2], three different cases and corresponding representative seastates were selected as summarized in Table 1. Case 1 evaluates fatigue limit state (FLS) during power production when the wind speed at hub height (U_w) is close to rated wind speed. Case 2 also evaluates FLS with the same structural and environmental inputs, but with the wind turbine in parked or idling case. The objective is to quantify how the significant loss of aerodynamic damping from Case 1 to Case 2 affects the sensitivity of fatigue loads with respect to input parameters. In addition, Case 3 is also evaluated to identify significant parameters under extreme environmental conditions. Co-directional and unidirectional wind and waves are assumed for all cases. Current loads are assumed to have insignificant effect. Eigenvalue and dynamic analyses are performed using the GBF model in HAWC2.

The aerodynamic loads in HAWC2 [23] are calculated based on Blade Element Momentum (BEM) theory [30,31]. The Mann turbulence model [32] is used to generate turbulent wind inputs (32 x 32 x 8192 points) at a timestep of 0.08 s. Normal and extreme turbulence are calculated assuming wind turbine Class III-C [1]. A power law wind profile with mean roughness (α) equal to 0.15 is assumed, which is typical for offshore sites [17,33].

The hydrodynamic loads are calculated based on Morison's equation [34,35]. It describes the total force per unit length as the sum of drag and inertia components as shown in Eq. (8), where D is the structure diameter, A is the cross-sectional area, ρ is the water density, and U and $\dot{U}$ are the wave particle velocity and acceleration, respectively. The drag (C_D) and inertia (C_M) coefficients are calibrated across the height of the GBF to account for diffraction and secondary steel. Based on model tests, the mean values of the coefficients $(C_D = 1.3, C_M = 2.0)$ are found. The linear irregular waves in HAWC2 are generated using an dynamic link library (DLL) file. Wave kinematics are based on JONSWAP spectrum with peak enhancement factor γ set to 3.3. Wheeler stretching is applied. In order to associate load variations to changes in input parameters, the same seed numbers are applied in generating wind and wave load inputs for all realizations. This avoids load variations due to the stochastic nature of environmental sea states.

$$F_{hydro} = \frac{1}{2}\rho C_D D U\left|U\right| + \rho C_M A\dot{U} \tag{8}$$

2.1.3. Fatigue damage assessment

Time-domain simulations of structural responses are performed based on the design load cases summarized in Table 1. Each realization of the time domain simulation is run for 600 s after transient responses at a timestep (Δt) of 0.02 s. From the resulting time series of loads, the load amplitudes and number of cycles were calculated using the standard rainflow procedure described by Amzallag [36]. The method is a widely used cycle-counting method for fatigue analysis of structures. The rainflow count algorithm used in Matlab was developed by Niesłony [37,38].

The fatigue damage is represented in terms of fatigue damage equivalent load, *DEL*, which when applied by N_{eq} cycles, generates the same amount of fatigue damage as the load history. The *DEL* for each realization can be calculated using the following expression:

$$DEL = \left(\frac{\sum_{i=1}^{N_c} n_i M_i^m p}{N_{eq}}\right)^{\frac{1}{m}} \tag{9}$$

where N_c is the total number of identified cycles in the load time series, n_i is the number of load cycles corresponding to the load magnitude M_i, m is the negative inverse slope of the S–N curve (also known as the Wöhler's exponent) taken as $m = 4$, N_{eq} is the reference number of cycles taken as $N_{eq} = 2.0\,E8$ for a design lifetime of 20 years, and p is the time scale factor calculated as the ratio between the total occurrence of a sea state throughout the design life and the simulation time. To ease comparison between the three defined load cases, each case is assumed to occur throughout the design lifetime $(p = 1.05\,E6)$, and the same damage assessment is done for Case 3 (ULS case). The equivalent load is calculated at the interface level $(DEL_{interface})$ and at the foundation base (DEL_{base}). The fatigue *DELs* can be used as damage indictors for steel and reinforcements, but results can be different for assessment of concrete fatigue damage. No safety factors are applied in the calculated loads.

The numerical model developed in HAWC2 is validated against load calculations from the detailed design of the Thornton Bank Offshore Wind Farm project.

Table 1
Description of design load cases.

Case No.	Load Case (Limit State)	U_w [m/s]	H_s [m/s]	T_p [s]	Turb. model
1	Power production (FLS)	12.0	1.55	5.2	Normal
2	Parked/Idling (FLS)	12.0	1.55	5.2	Normal
3	Parked/Idling (ULS)	42.0	6.10	11.0	Extreme

2.2. Sensitivity analysis

The primary objective of performing a sensitivity analysis (SA) on a numerical model is to assess the relative importance of input parameters (X) in determining the model outputs $(Y = f(X))$. A common method for SA is the one-factor-at-a-time (OAT) approach, where a parameter is pertubated while keeping all the other factors fixed at nominal values. This approach, however, leads to conclusions that are limited within the local sampling space and are only valid if the model is proven to be linear [39]. For highly nonlinear systems, such as load analysis of offshore wind turbines, global SA methods can provide better linearization of non-linear models over the entire range of input parameters [20].

This section discusses the two global SA approaches applied, namely the (1) linear regression of Monte Carlo simulations, also known as *Standardized Regression Coefficients (SRC)* method, and the (2) Morris Screening method. The algorithms and general workflow for both methods are adopted from Sin et al. [40] as illustrated in Fig. 4. The procedure for both methods are similar, with the main difference coming from the sampling strategy and calculation of sensitivity indices.

Simulations performed for both SRC method and Morris Screening are based on the time-domain coupled dynamic analysis of the GBF model discussed in the preceeding section. The last part of this section presents the input parameters relevant for numerical simulation of offshore wind turbine loads.

2.2.1. Linear regression of Monte Carlo simulations

The Monte Carlo (MC) method [41] is a common technique used to obtain numerical solutions to multi-dimensional integrals, which are difficult or impossible to solve analytically. A stochastic input variable $x = [z_1, z_2, .., z_m]$ with m model inputs (z_i) is sampled independently based on the defined distributions and uncertainties. The solution (Y) to the multi-dimensional integral function $(f(x))$ over the unit hypercube $[0, 1]^m$ can be expressed as shown in Eq. (10). Based on the law of large numbers, a high number of model realizations (N) result to the MC estimate $(E[Y])$ to converge to Y [40].

$$Y = \int f(x)\, d^m x \tag{10}$$

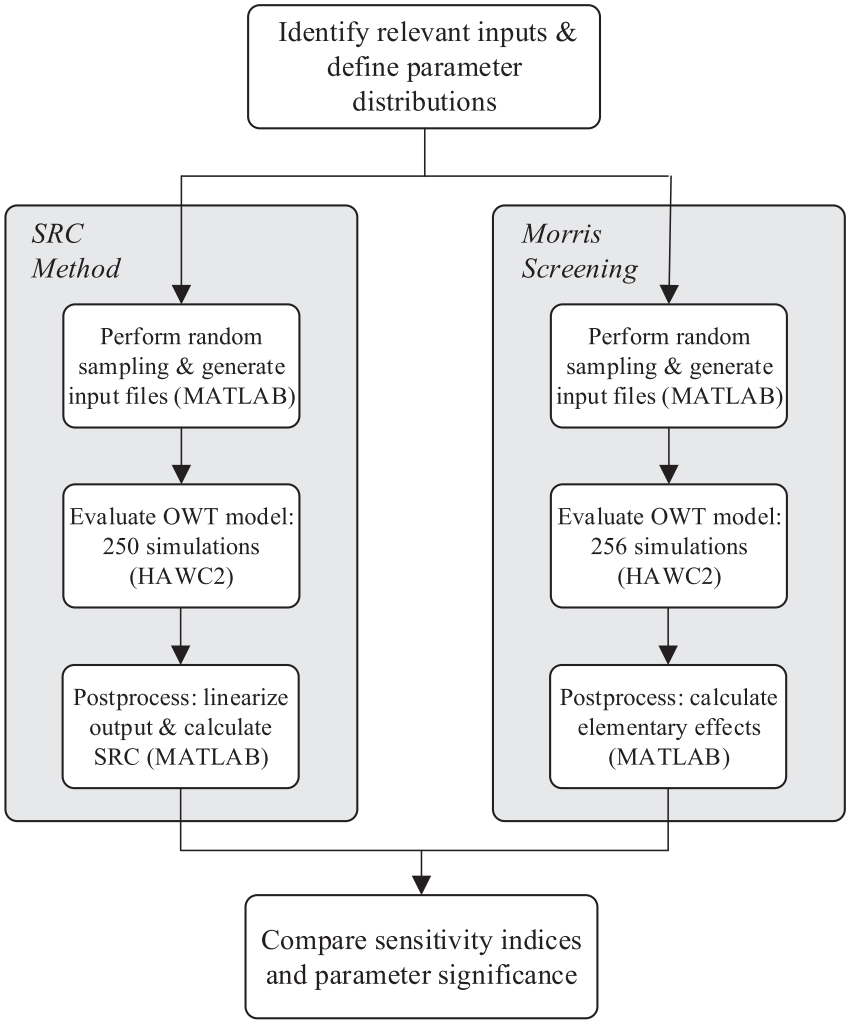

Fig. 4. General workflow for sensitivity analysis.

$$\lim_{N\to\infty}\frac{1}{N}\sum_{j=1}^{N}f(x_j)=Y \tag{11}$$

$$E[Y]=\frac{1}{N}\sum_{j=1}^{N}f(x_j) \tag{12}$$

A simple linear regression of Monte Carlo simulations [5], can be performed to obtain a linear model (y) as a function of each model inputs:

$$y=a+\sum_{i=1}^{m}b_i z_i \tag{13}$$

where a and b_i are the y-intercept and regression coefficients, respectively, which are determined by least squares method. The standardized regression coefficients (β_i) can be calculated by normalizing the regression coefficients (b_i) using the standard deviations of model input (σ_{x_i}) and output (σ_y) as follows:

$$\beta_i=b_i\,\frac{\sigma_{x_i}}{\sigma_y} \tag{14}$$

The sensitivity measure β_i can be any value from $[-1,1]$. A high absolute value indicates significant effect, while a value close to zero indicates insignificant effect from the input parameter. Further, a positive value indicates a positive effect (and vice versa). In cases when the model is fully linear, β_i^2 corresponds to the relative variance contributions of model inputs to the model output variance, and it follows that $\sum_{i=1}^{m}\beta_i^2=1$. In this case, β_i^2 coincides with the 1st order sensitivity index or main effect index (S_i). The validity of β_i as a sensitivity measure can be determined by calculating the model coefficient of determination (R^2), which indicates the fraction of the output variance that can be explained by the linear model. R^2 is calculated from the correlation coefficient (R) for a given Monte Carlo output (y') and linear model estimate (y) as:

$$R=\frac{N\sum yy'-\sum y\sum y'}{\sqrt{\left[N\sum y^2-(\sum y)^2\right]\left[N\sum y'^2-(\sum y')^2\right]}} \tag{15}$$

Typically, a value of $R^2\geq 0.70$ indicates that a linear model assumption is sufficient [4,42,43]. A total of $N_{MC}=250$ Monte Carlo simulations were run for each case.

2.2.2. Morris Screening

Morris Screening [6], also known as *Elementary Effects* method, is an efficient method for identifying important parameters in computationally expensive numerical models with numerous factors. Although the method is based on randomized one-factor-at-a-time (OAT) approach, it overcomes the main limitation related to local variation by introducing a sampling strategy that allows a "global" variation in the model input. The proposed method by Morris [6] aims to predict whether an input is (a) negligible, (b) linear and additive, or (c) nonlinear or has a interactions with other parameters.

Independent random sampling for k independent model inputs is performed within the input region (Ω), defined as a k-dimensional unit hypercube with p-level grids. Factors are initially assumed to be uniformly distributed over $[0,1]$, before being transformed to their actual distributions. In order to calculate one *Elementary Effect* (EE), a minimum of two model evaluations has to be performed: one at the randomly sampled input variables $(\mathbf{x}\in\Omega)$, and one after increasing x_i with Δ, a predetermined increment which may take a value of $[0,1]$ at multiples of $1/(p-1)$ such that the transformed input is still within the input region $(\mathbf{x}_{x_i+\Delta}\in\Omega)$. The EE_i, which quantifies the change in output (y) due to a incremental change Δ in a particular input (X_i), is defined in Eq. (16). The EE_i definition [6] is modified to obtain a non-dimensional (σ-scaled) sensitivity measure.

$$EE_i=\frac{[y(x_1,x_2,\cdots,x_{i-1},x_i+\Delta,x_{i+1},\cdots,x_k)-y(\mathbf{x})]}{\Delta}\;\frac{\sigma_{x_i}}{\sigma_y} \tag{16}$$

In the sampling strategy proposed by Morris, each model

Table 2
Parameter distributions for structural and soil input parameters.

Parameter	Unit	Dist.	Mean	COV	Source	Notes
E_s	[MPa]	LN	2.10E+05	0.03	[45,46]	Steel E-mod.
E_c	[MPa]	N	2.96E+04	0.06	[47,48]	Concrete E-mod.
$M_{nacelle}$	[kg]	N	2.95E+05	0.025	[a]	Nacelle mass
M_{hub}	[kg]	N	7.00E+04	0.025	[a]	Hub mass
t_{dev}	[mm]	N	1	0.66	[49]	Tower thickness tolerance
ζ	[%]	LN	1.1	0.1	[26,28],[a]	Damping ratio
G_{soil}	[MPa]	U	110.0	0.32	[13,50]	Range: 50 MPa - 170 MPa
ν_{soil}	[−]	U	0.3	0.10	[50],[a]	Range: 0.25–0.35

[a] Expert opinion/available data.

Table 3
Parameter distributions for metocean inputs.

Parameter	Unit	Dist.	Cases 1 & 2		Case 3		Source	Notes
			Mean	COV	Mean	COV		
U_w	[m/s]	N	12	0.05	42	0.012	[51],[a]	Mean at hub
TI	[−]	LN	0.146	0.200	0.11	0.100	[17,33,52,53]	–
α	[−]	LN	0.150	0.667	0.15	0.180	[17,33]	–
H_s	[m]	LN	1.55	0.065	6.1	0.065	[51,54]	–
T_p	[s]	LN	5.2	0.038	11	0.038	[51,54]	–
h	[m]	LN	25.0	0.03	25.0	0.03	[a]	–
f_{wave}	[−]	U	1.50	0.19	1.50	0.19	[15],[a]	1.0–2.0 (load factor)

[a] Expert opinion/available data.

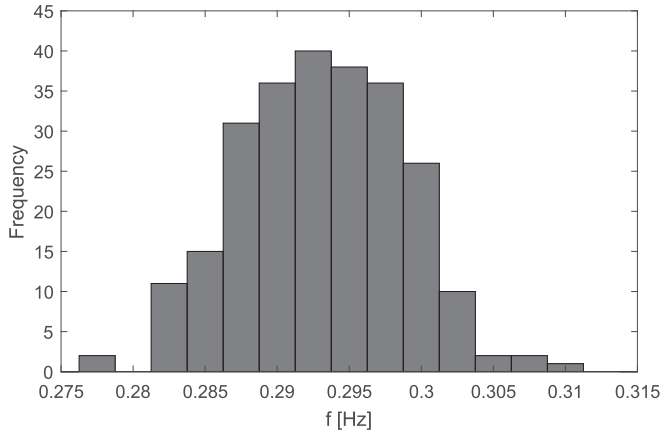

Fig. 5. Histogram of calculated f_{nat}.

evaluations (except the first row) are used to calculate two *EEs*. The total number of evaluations (n) is given by $n = r(k+1)$, where the number of trajectories (r) is normally between 10 and 50 [44]. In this study, 16 trajectories for $k = 15$ parameters results to a total of $N_{Morris} = 256$ evaluations for each case, sampled at $p = 6$ levels. A full description of the method can be found in Morris [6] and Campolongo & Saltelli [43].

After HAWC2 model evaluations are performed n times, two sensitivity measures can be calculated for each input: the mean (μ) and standard deviation (σ) of the *EEs* distribution as shown in Eq. (17) and Eq. (18), respectively. A high absolute μ value indicates that an input has an significant overall effect on the output, while a high σ indicates that the input has a nonlinear effect or interactions with other factors. Both μ and σ are important indicators to consider in parameter significance ranking and are normally represented graphically by plotting both indices on the x and y axes, respectively. In general, if the coordinates (μ_i, σ_i) of a factor lie outside the wedge formed by $d_i = \pm 2\, SEM_i$, where $SEM_i = \sigma_i/\sqrt{r}$, the parameter is significant [6].

$$\mu_i = \frac{1}{r}\sum_{i=1}^{r} EE_i \tag{17}$$

$$\sigma_i = \sqrt{\frac{1}{r}\sum_{1}^{r}(EE_i - \mu_i)^2} \tag{18}$$

For models with very large number of model inputs, the use of Morris's indices (μ_i, σ_i) becomes problematic due to large number of factors and the method becomes more vulnerable to Type II error (failure to identify influential factors) [4]. An alternative option is to calculate the refined mean index (μ_i^*) proposed by Campolongo et al. [44]. It has been shown that μ_i^* is an effective substitute for the total sensitivity index S_T for less computational expense.

2.2.3. Parameter uncertainties

Integrated fatigue analysis of OWT structures requires a high number of parameters to define the structural, geotechnical and environmental submodels. In performing a global SA, it is important to define the parameter distributions as accurately as possible, since the results are interpreted based on the input uncertainties.

Table 2 summarizes the structural and soil input distributions, which are used for eigenvalue analysis. Table 3 summarizes metocean input distributions, which are used in dynamic analysis together with the inputs from Table 2. All parameters are assumed independent (no correlation), which is acceptable for lumped sea states. The assessment of uncertainties are based on existing literature, available data and expert opinion. Both SRC method and Morris Screening used the same sets of parameter distributions.

Due to high computational requirements and several cases considered, the sensitivity of the results to the number of simulations was not investigated. Clearly, performing more simulations would improve convergence and increase the accuracy of the results. The ideal number of realizations varies from model to model, and is normally influenced by the computational requirements and the number of model parameters. A good practice is to make sure that the sampling sufficiently covers the possible range of values for each model parameters, which can be done by investigating the scatter plots.

3. Results and discussion

The sensitivity of three model outputs, namely the 1st fore-aft natural frequency f_{nat} and equivalent loads at the foundation $DEL_{interface}$ and base DEL_{base}, are presented in this section. The

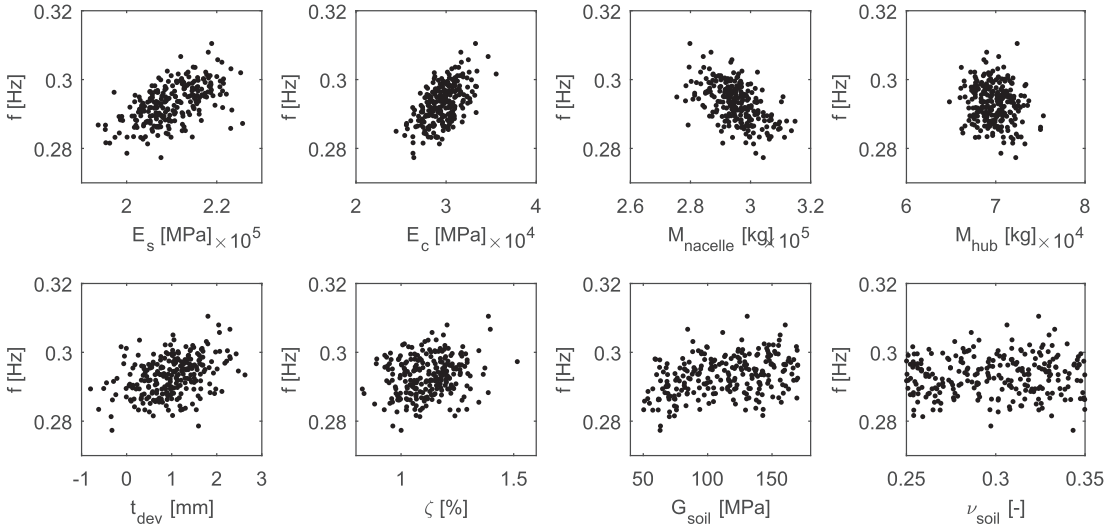

Fig. 6. Scatter plots for structural & soil input parameters and f_{nat}.

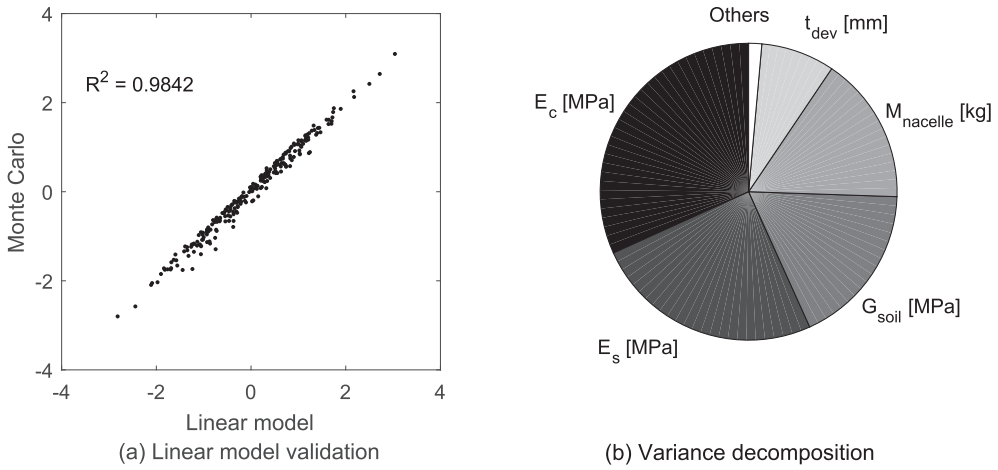

Fig. 7. Monte Carlo-based (a) linear model and (b) variance decomposition for f_{nat} [*Hz*].

results are organized into three parts. The first and second subsections present the analyses from the SRC method and Morris screening, respectively. The last subsection compares the sensitivity indices based on the two methods and summarizes parameter significance rankings.

3.1. SRC method

3.1.1. Eigenvalue analysis

The resulting distribution of the f_{nat} is shown in Fig. 5, which indicates that a small variance exists. A mean value of 0.2931 *Hz* and a standard deviation of 0.0056 result to a $COV_{f_{nat}} = 0.019$. Visual observation of the scatter plot, shown in Fig. 6, also provides insights on which uncertain parameters affect the f_{nat}. An increase in $M_{nacelle}$, for instance, generally reduces the f_{nat}. Positive and negative correlations are associated with positive and negative values of $\beta's$, respectively.

The fitted linear regression model is shown in Fig. 7a, which predicts the f_{nat} as a linear function of the soil and structural input parameters. The linear model predicts with an accuracy of $R^2 = 0.98$. Having $R^2 > 0.70$ suggests that $\beta's$ are statistically valid sensitivity indices. The variance decomposition, shown in Fig. 7b, indicates how much each of the most significant parameters (E_c, E_s, G_{soil}, $M_{nacelle}$ and t_{dev}) contribute to the total variance in f_{nat} that can be explained by the linear model. An accurate prediction of the f_{nat} is primarily important in preliminary designs, where the support structure is configured such that the f_{nat} do not to coincide with the environmental load spectrum. The calculated sensitivity indices ($\beta's$) are compared to the Morris's elementary effects ($EE's$) in the succeeding subsection.

3.1.2. Dynamic analysis

The distribution of $DEL_{interface}$ and DEL_{base}, which are separately normalized with respect to the maximum value of the three load cases considered, are shown in Fig. 8. In general, a higher variance is observed in Case 3 (ULS case) as compared to Cases 1 and 2. Fatigue equivalent loads also exhibit higher uncertainty during parked or idling condition (Case 2) relative to operating condition (Case 1). Relative to Case 1, the Case 2 $DEL_{interface}$ and DEL_{base} standard deviations increased by 46% and 19%, respectively. Coefficient of

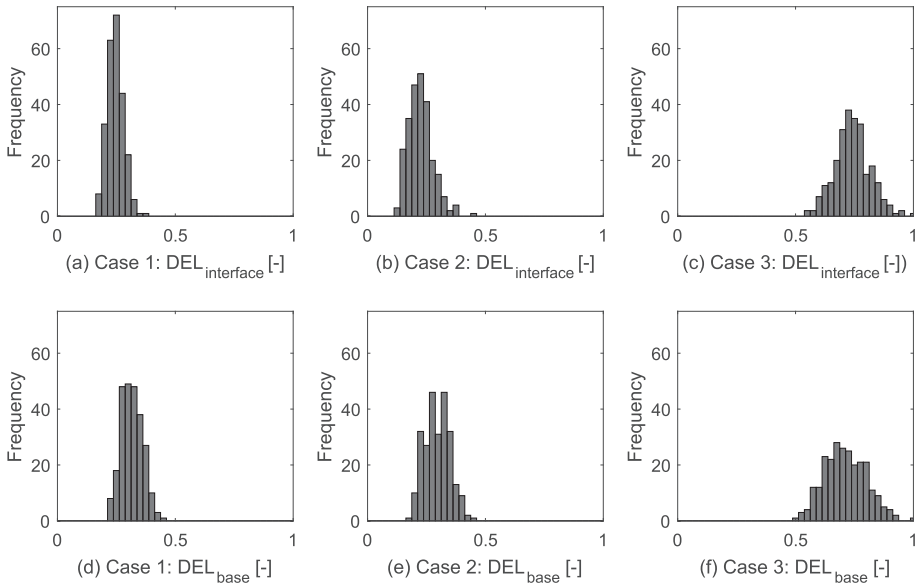

Fig. 8. Histogram of calculated $DEL_{interface}$ and DEL_{base} at load cases 1, 2 and 3.

Table 4
Coefficient of variation (cov) for $DEL_{interface}$ and DEL_{base}.

Case 1	Case 2	Case 3
0.144	0.232	0.101
0.140	0.177	0.125

variations for different cases are summarized in Table 4. For the total fatigue calculation, contributions from Case 2 are limited relative to Case 1 contributions.

For the fatigue analysis, the 15 stochastic input parameters resulted in high output variance. In order to recognize correlation, the output has to be arranged according to the parameter which has the largest main effect or nonlinear effect. A scatter plot with selected parameters (f_{wave}, TI, G_{soil}) are shown in Fig. 9. The wave load factor (f_{wave}) and turbulence intensity (TI) show strong positive correlations, particularly at the DEL_{base} and $DEL_{interface}$, respectively. The plots also imply that parameter sensitivity of the same output can vary depending on the load case. Considering $DEL_{interface}$, Case 2 is less significant to TI but tends to be more sensitive to f_{wave} and G_{soil}. A nonlinear pattern can also be distinguished in G_{soil}, where both DEL_{base} and $DEL_{interface}$ tend to increase in magnitude as G_{soil} approaches the lower limits or softer soil

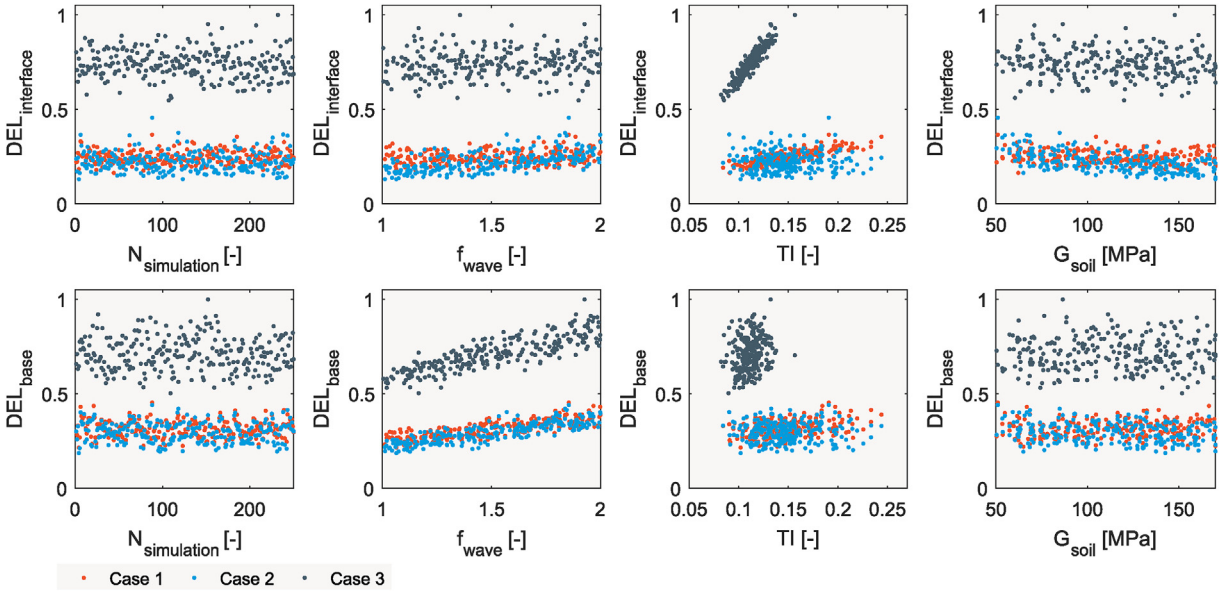

Fig. 9. Scatter plots for selected input parameters at $DEL_{interface}$ and DEL_{base}.

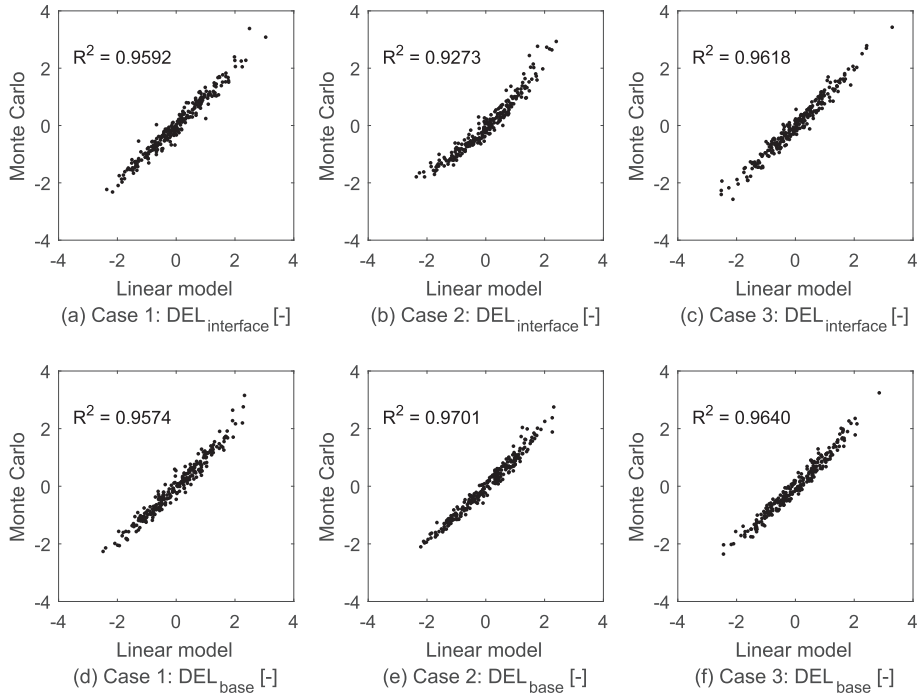

Fig. 10. Monte Carlo-based linear models for DEL at interface and base.

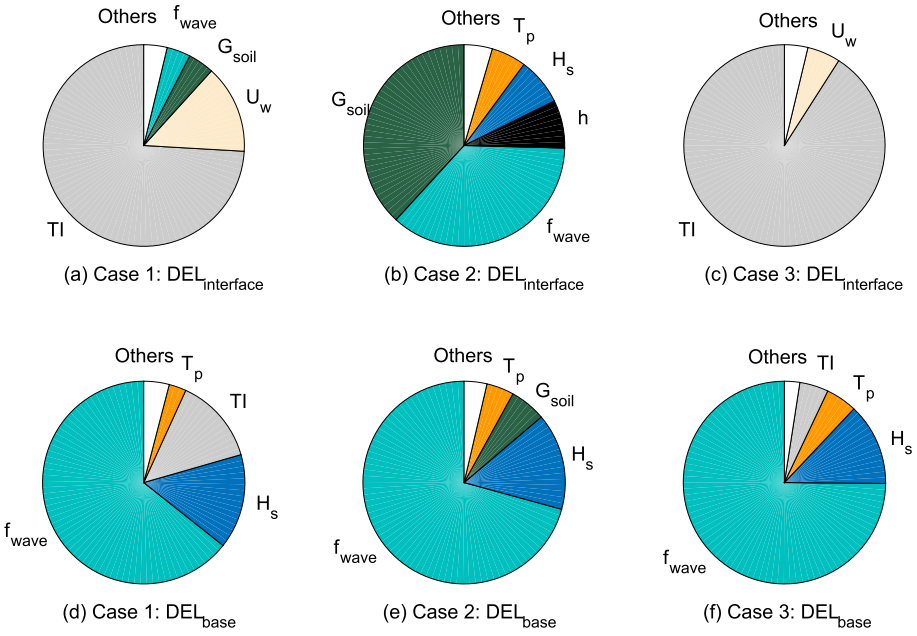

Fig. 11. Variance decomposition for DEL at interface and base.

conditions.

The fitted linear regression models for fatigue *DELs* are shown in Fig. 10. Similarly, the linear models have satisfactory $R^2 > 0.70$, which indicates that the sensitivity indices $\beta's$ are reliable metrics. Consequently, the corresponding variance decomposition are illustrated in Fig. 11. The following conclusions can be made based on Fig. 11:

- Generally, uncertainties from environmental and soil input parameters are more significant than structural inputs
- The $DEL_{interface}$ is highly influenced by *TI*, except during idling case where G_{soil} and f_{wave} become the dominant input parameters.
- The DEL_{base} is highly influenced by f_{wave} in all cases. The idling case also makes G_{soil} an important parameter.
- For both $DEL_{interface}$ and DEL_{base}, *TI* has reduced significance during FLS at the idling case, where the blades are pitched and aerodynamic loads are greatly reduced.
- For the idling case (Case 2), the higher output variance of $DEL_{interface}$ relative to Case 1 can be explained by parameters G_{soil} and f_{wave} that become more significant (see Fig. 9). Higher *DELs* occur at high f_{wave} and low G_{soil} (soft soil), while lower *DELs* occur at low f_{wave} and high G_{soil} (stiff soil). This interaction between soil and wave parameters causes higher uncertainty in loads during the idling case.

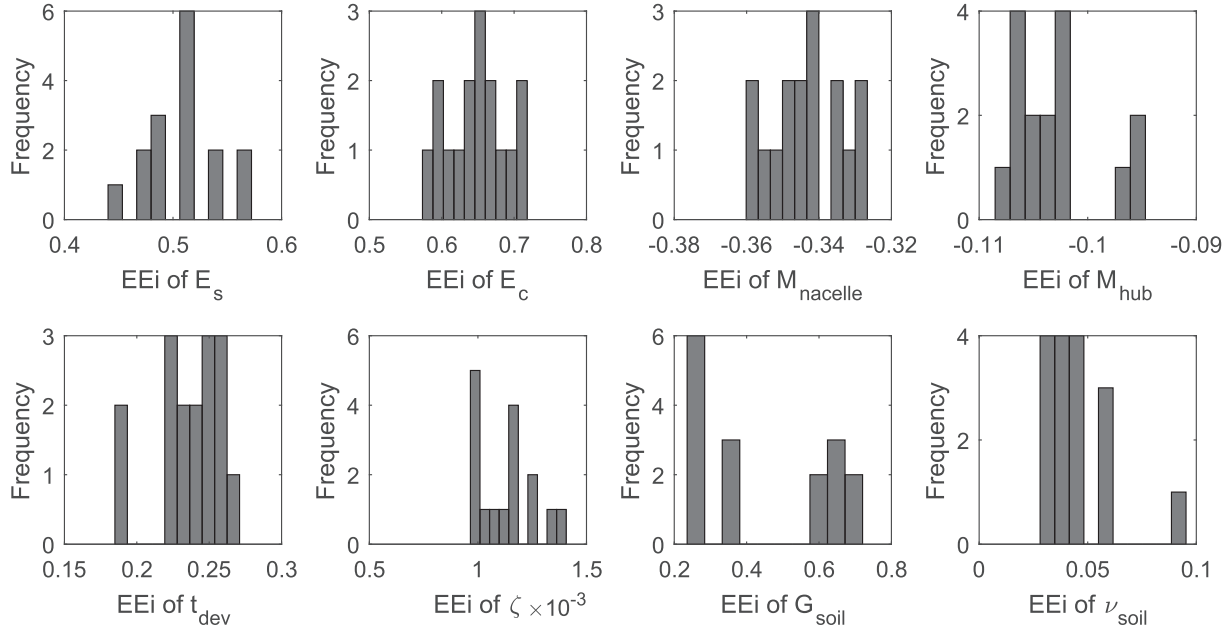

Fig. 12. Elementary effects distribution of soil and structural parameters for f_{nat}.

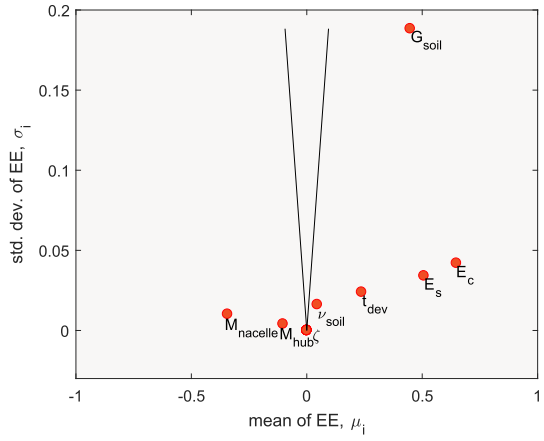

Fig. 13. Mean and standard deviation of sigma-scaled elementary effects distribution for f_{nat} with lines ± 2*SEM.

The calculated sensitivity indices ($\beta's$) are compared to the Morris's elementary effects ($EE's$) in the succeeding subsection.

3.2. Morris screening method (elementary effects)

3.2.1. Eigenvalue analysis

The resulting elementary effects ($EE's$) distribution, which has a total of 16 trajectories per input parameter, are shown in Fig. 12. If a parameter has no influence on the output, all the calculated $EE's$ would be zero.

The sensitivity indices of each input parameter can be derived from the $EE's$ distribution by calculating the mean (μ) and the standard deviation (σ). The indices are graphically represented in Fig. 13 and the location of each point indicates the importance of the parameter. Parameters that lie outside the wedge formed by the lines $+/-2{*}SEM$ are generally important. The μ relates to the main effect, which means parameters that are far from zero are generally significant. A negative μ indicates negative main effect, i.e. an increase in $M_{nacelle}$ generally decreases f_{nat}. The σ, on the other hand, indicates interactive or non-linear effect. The G_{soil} appeared to have a relatively strong interactive or non-linear effect on the f_{nat}. This agrees well with the scatter plot presented in Fig. 6, which shows that the f_{nat} is generally not sensitive to G_{soil} until it reaches a very low value ($G_{soil} \approx 50$ *to* $65\ MPa$) where f_{nat} can be significantly reduced (nonlinear effect). For f_{nat}, the factors that are identified as significant by Morris screening generally agree with the results from the SRC method.

3.2.2. Dynamic analysis

The sensitivity indices for the $DEL_{interface}$ and DEL_{base} are calculated for Cases 1, 2 and 3 as illustrated in Fig. 14. Direct case comparisons with the results from SRC method (see Fig. 11) suggest that there is good agreement with the reported parameter importance. In addition, results from Morris screening has verified interactive or non-linear effects of G_{soil}, which can only be deduced in SRC method by investigation of scatter plots. Hübler et al. [20], who conducted sensitivity analysis of an OWT supported by monopile and jacket support structures, also concluded that soil parameters have significant interaction effects.

3.3. Comparison of SA method

The results of the SRC method and Morris screening are compared by summarizing the sensitivity indices according to main effect (β_i, μ_i). Parameter significance rankings for f_{nat}, $DEL_{interface}$, and DEL_{base} are listed in Tables 5–7, respectively. Both methods ranked the f_{nat} inputs in the same order of importance. Rankings for $DEL_{interface}$ and DEL_{base} are also in good agreement, and only starts to differ at the least significant parameters. The similarity in the sensitivity indices (β_i, μ_i) is not a coincidence, since both are effective approximations of the total sensitivity index (S_{T_i}) at a much lower computational cost [4].

For the SRC method, the $\sum_{i=1}^{N}\beta_i^2$ are also calculated to check consistency of the linear regression. In theory, $\sum_{i=1}^{N}\beta_i^2 = R^2$ if the regression resulted to a fully linear relation. For f_{nat}, having $\sum_{i=1}^{N}\beta_i^2 = 85.7\%$ and $R^2 = 0.98$ suggests that f_{nat} is not a fully linear output. Nonetheless, even for nonlinear models, the $\beta's$ remain

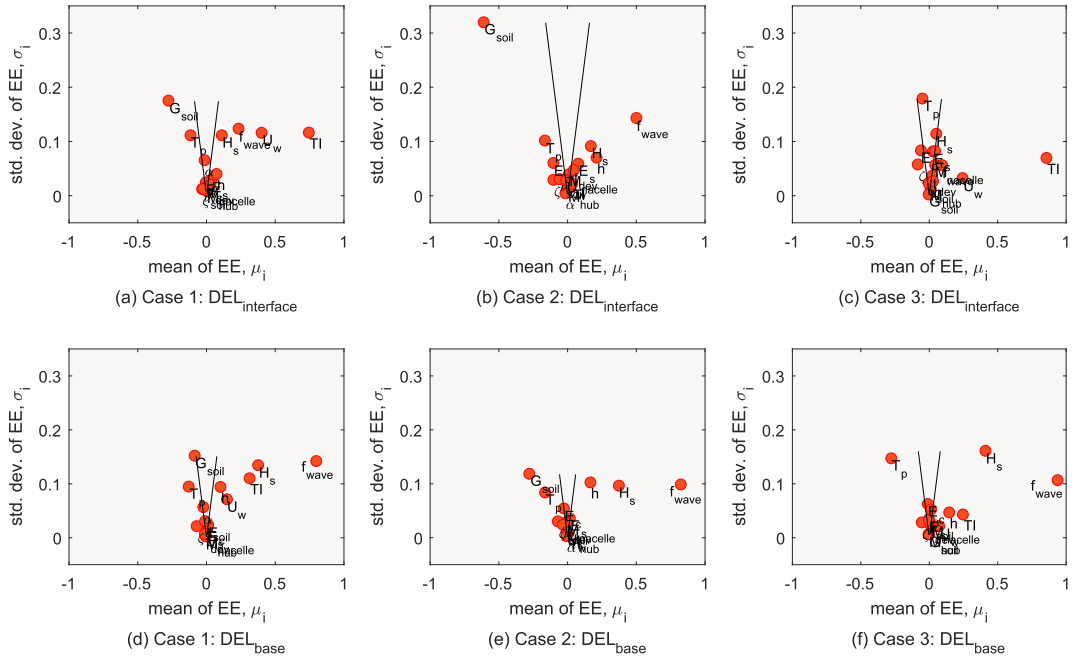

Fig. 14. Mean and standard deviation of sigma-scaled elementary effects distribution for $DEL_{interface}$ and DEL_{base} with lines ± 2*SEM.

Table 5
Summary of sensitivity indices for eigenvalue analysis.

Rank	Monte Carlo		Morris Method	
	Input	β	Input	μ
1	E_c	0.522	E_c	0.648
2	E_s	0.463	E_s	0.507
3	G_{soil}	0.390	G_{soil}	0.448
4	M_{nac}	−0.371	M_{nac}	−0.343
5	t_{dev}	0.262	t_{dev}	0.237
6	M_{hub}	−0.101	M_{hub}	−0.103
7	ν	0.042	ν	0.045
8	ζ	0.017	ζ	0.001
$\sum_{i=1}^{N_{par}} \beta_i^2$		0.857		

reliable sensitivity measures since it is derived from the entire input space, and thus represents the global or multi-dimensionally averaged values [4]. In addition, having $R^2 > 0.70$ and $\sum_{i=1}^{N} \beta_i > 0.70$ suggest that $\beta's$ are still statistically valid sensitivity indices, and conclusions shall be drawn while bearing in mind that about 15% of the variation inf f_{nat} is not explained by the model. For the dynamic analysis, the $\sum_{i=1}^{N} \beta_i$ values are very close to the R^2 values. The small differences arise from numerical approximations and from the fact that the output is not perfectly linear.

4. Conclusions

This study demonstrated two effective global SA methods to determine the sensitivity of OWT fatigue loads to structural, soil and environmental inputs. Parameters with main and nonlinear effects were identified, and it was found that the set of influential parameters vary according to which design load case is considered. Parameter significance rankings given by the SRC method and Morris screening are in good agreement.

Fatigue loads are found to be more sensitive to uncertainties in wind, wave and soil parameters as compared to uncertainties in structural inputs. In particular, damage equivalent loads at the foundation-tower interface ($DEL_{interface}$) are mostly influenced by turbulence intensity (TI) during power production (Case 1) and extreme conditions (Case 3). During parked or idling conditions (Case 2), the soil shear stiffness (G_{soil}) and wave load factor (f_{wave})

Table 6
Summary of sensitivity indices for DEL at support structure interface.

Rank	Case 1				Case 2				Case 3			
	Monte Carlo		Morris Method		Monte Carlo		Morris Method		Monte Carlo		Morris Method	
	Input	β	Input	μ	Input	β	Input	μ	Input	β	Input	μ
1	TI	0.846	TI	0.749	G_{soil}	−0.601	G_{soil}	−0.606	TI	0.963	TI	0.860
2	U_w	0.370	U_w	0.405	f_{wave}	0.586	f_{wave}	0.505	U_w	0.233	U_w	0.247
3	G_{soil}	−0.201	G_{soil}	−0.272	h	0.270	h	0.215	f_{wave}	0.093	f_{wave}	0.098
4	f_{wave}	0.192	f_{wave}	0.238	H_s	0.267	H_s	0.173	G_{soil}	−0.090	ζ	−0.080
5	H_s	0.110	H_s	0.116	T_p	−0.230	T_p	−0.161	M_{nac}	0.085	E_c	−0.057
6	T_p	−0.105	T_p	−0.112	ζ	−0.154	E_c	−0.099	ζ	−0.082	H_s	0.055
7	h	0.076	h	0.078	E_s	0.077	ζ	−0.099	H_s	0.040	M_{nac}	0.047
8	E_s	0.054	E_s	0.043	ν	−0.068	E_s	0.082	T_p	−0.040	α	−0.047
9	ζ	−0.049	t_{dev}	0.033	E_c	−0.064	ν	−0.055	E_c	0.039	T_p	−0.046
10	α	−0.026	ζ	−0.028	TI	0.046	t_{dev}	0.050	h	0.032	h	0.032
11	t_{dev}	0.025	ν	−0.020	α	−0.030	TI	0.037	α	0.028	E_s	0.031
12	M_{nac}	0.019	α	−0.009	M_{nac}	0.024	M_{nac}	0.013	ν	−0.024	t_{dev}	0.025
13	E_c	0.016	M_{nac}	0.007	U_w	−0.020	α	−0.012	t_{dev}	0.021	M_{hub}	0.012
14	ν	−0.014	M_{hub}	0.003	t_{dev}	0.018	M_{hub}	0.006	E_s	0.012	ν	0.000
15	M_{hub}	0.004	E_c	−0.001	M_{hub}	0.013	U_w	−0.006	M_{hub}	0.008	G_{soil}	0.000
$\sum_{i=1}^{N_{par}} \beta_i^2$		0.965				0.944				1.020		

Table 7
Summary of sensitivity indices for DEL at foundation base.

Rank	Case 1				Case 2				Case 3			
	Monte Carlo		Morris Method		Monte Carlo		Morris Method		Monte Carlo		Morris Method	
	Input	β	Input	μ	Input	β	Input	μ	Input	β	Input	μ
1	f_{wave}	0.789	f_{wave}	0.803	f_{wave}	0.835	f_{wave}	0.828	f_{wave}	0.840	f_{wave}	0.942
2	H_s	0.383	H_s	0.380	H_s	0.390	H_s	0.378	H_s	0.352	H_s	0.415
3	TI	0.365	TI	0.318	G_{soil}	−0.239	G_{soil}	−0.274	T_p	−0.217	T_p	−0.273
4	T_p	−0.163	U_w	0.153	T_p	−0.208	h	0.171	TI	0.208	TI	0.250
5	h	0.141	T_p	−0.125	h	0.174	T_p	−0.159	h	0.124	h	0.150
6	U_w	0.116	h	0.106	ζ	−0.060	ζ	−0.067	G_{soil}	−0.055	U_w	0.077
7	ζ	−0.063	G_{soil}	−0.082	ν	−0.031	ν	−0.029	U_w	0.048	ζ	−0.051
8	E_s	0.026	ζ	−0.067	E_s	0.023	E_c	−0.023	ζ	−0.033	α	0.017
9	t_{dev}	−0.023	α	−0.019	α	−0.014	E_s	0.021	M_{nac}	0.024	M_{nac}	0.015
10	E_c	0.019	E_c	0.016	E_c	−0.007	TI	0.010	M_{hub}	0.021	t_{dev}	0.010
11	G_{soil}	0.016	t_{dev}	−0.007	U_w	−0.005	M_{nac}	−0.009	E_s	0.011	E_c	−0.007
12	α	0.009	E_s	0.006	TI	0.004	t_{dev}	0.008	t_{dev}	−0.006	M_{hub}	0.003
13	M_{hub}	0.008	ν	−0.006	M_{hub}	−0.004	α	−0.004	ν	−0.006	ν	0.002
14	M_{nac}	0.006	M_{nac}	−0.002	M_{nac}	−0.003	U_w	−0.002	E_c	0.006	G_{soil}	−0.001
15	ν	0.003	M_{hub}	−0.001	t_{dev}	−0.001	M_{hub}	0.002	α	0.005	E_s	0.001
$\sum_{i=1}^{N_{par}} \beta_i^2$		0.968				0.985				0.944		

become the most important parameters for $DEL_{interface}$. Damage equivalent loads at the foundation base (DEL_{base}) are mostly influenced by f_{wave}, followed by the significant wave height (H_s) for all cases. Both methods also suggest that the variation in G_{soil} causes significant nonlinear or interaction effects for both $DEL_{interface}$ and DEL_{base} during fatigue design load Case 2, and also to a certain extent for Case 1.

Finally, the results can vary depending on the foundation design, wind turbine size, design load case and site-specific environmental conditions. Further studies involving wind-wave misalignment, improved foundation and wave modeling, more extensive range of environmental conditions, and comparison between different types of foundations can be pursued. Nonetheless, this study provides insights to foundation designers and wind turbine manufacturers on which parameters must be assessed in more detail in order to reduce uncertainties in load prediction.

Acknowledgements

This research work was performed within the European project INFRASTAR, which has received funding from the European Union's Horizon 2020 research and innovation programme under the Marie Skłodowska-Curie grant agreement No 676139.

References

[1] International Electrotechnical Commission, et al., IEC 61400-1: wind turbines part 1: design requirements, in: International Electrotechnical Commission, 2005.
[2] International Electrotechnical Commission, et al., IEC 61400-3: wind turbines part 3 - design requirements for offshore wind turbines, Wind Turbines-Part 3 (2009).
[3] Design of Offshore Wind Turbine Structures (DNV-OS-J101), DET NORSKE VERITAS, 2014.
[4] Andrea Saltelli, et al., Global Sensitivity Analysis: the Primer, John Wiley & Sons, 2008.
[5] Jon C. Helton, Freddie Joe Davis, Latin hypercube sampling and the propagation of uncertainty in analyses of complex systems, Reliab. Eng. Syst. Saf. 81 (1) (2003) 23–69.
[6] Max D. Morris, Factorial sampling plans for preliminary computational experiments, Technometrics 33 (2) (1991) 161–174.
[7] Kok-Kwang Phoon, Fred H. Kulhawy, Characterization of geotechnical variability, Can. Geotech. J. 36 (4) (1999) 612–624.
[8] Kok-Kwang Phoon, Fred H. Kulhawy, Evaluation of geotechnical property variability, Can. Geotech. J. 36 (4) (1999) 625–639.
[9] M.B. Zaaijer, Foundation modelling to assess dynamic behaviour of offshore wind turbines, Appl. Ocean Res. 28 (1) (2006) 45–57.
[10] Sumanta Haldar, GL Sivakumar Babu, Effect of soil spatial variability on the response of laterally loaded pile in undrained clay, Comput. Geotech. 35 (4) (2008) 537–547.
[11] Mohammad Javad Vahdatirad, et al., in: Probabilistic Three-Dimensional Model of an Offshore Monopile Foundation: Reliability Based Approach, 2013.
[12] Wystan Carswell, et al., Soil-structure reliability of offshore wind turbine monopile foundations, Wind Energy 18 (3) (2015) 483–498.
[13] Mads Damgaard, et al., A probabilistic analysis of the dynamic response of monopile foundations: soil variability and its consequences, Probabilist. Eng. Mech. 41 (2015) 46–59.
[14] Fabian Vorpahl, et al., Offshore wind turbine environment, loads, simulation, and design, Wiley Interdiscip. Rev. Energy Environ. 2 (5) (2013) 548–570.
[15] Amy N. Robertson, et al., OC5 Project Phase Ib: validation of hydrodynamic loading on a fixed, flexible cylinder for offshore wind applications, Energy Procedia 94 (2016) 82–101.
[16] Ana Glisic, Goncalo T. Ferraz, Peter Schaumann, et al., Sensitivity analysis of monopiles' fatigue stresses to site conditions using Monte Carlo simulation, in: The 27th International Ocean and Polar Engineering Conference, International Society of Offshore and Polar Engineers, 2017.
[17] Henrik Stensgaard Toft, et al., Uncertainty in wind climate parameters and their influence on wind turbine fatigue loads, Renew. Energy 90 (2016) 352–361.
[18] Henrik Stensgaard Toft, et al., Wind climate parameters for wind turbine fatigue load assessment, J. Solar Energy Eng. 138 (3) (2016) 031010.
[19] Juan Pablo Murcia, et al., Uncertainty propagation through an aeroelastic wind turbine model using polynomial surrogates, Renew. Energy 119 (2018) 910–922.
[20] Clemens Hubler, Cristian Guillermo Gebhardt, Raimund Rolfes, Hierarchical four-step global sensitivity analysis of offshore wind turbines based on aeroelastic time domain simulations, Renew. Energy 111 (2017) 878–891.
[21] Rebecca Martin, et al., Sensitivity analysis of offshore wind farm operation and maintenance cost and availability, Renew. Energy 85 (2016) 1226–1236.
[22] Lisa Ziegler, Michael Muskulus, Fatigue reassessment for lifetime extension of offshore wind monopile substructures, J. Phys. Conf. Series 753 (9) (2016) 092010. IOP Publishing.
[23] Torben J. Larsen, Anders Melchior Hansen, How 2 HAWC2, the User's Manual. Tech. Rep, Riso National Laboratory, 2015.
[24] Jason Jonkman, et al., Definition of a 5-MW Reference Wind Turbine for Offshore System Development, Tech. Rep., National Renewable Energy Laboratory (NREL), Golden, CO., 2009.
[25] W. Carswell, et al., Foundation damping and the dynamics of offshore wind turbine monopiles, Renew. Energy 80 (2015) 724–736.
[26] R. Shirzadeh, et al., Experimental and computational damping estimation of an offshore wind turbine on a monopile foundation, J. Wind Eng. Indus. Aerodyn. 120 (2013) 96–106.
[27] Lord Rayleigh, Theory of Sound (Two Volumes, Dover Publications, New York, 1897.
[28] Christof Devriendt, et al., Damping estimation of an offshore wind turbine on a monopile foundation, IET Renew. Power Gen. 7 (4) (2013) 401–412.
[29] Erica Bush, Lance Manuel, The influence of foundation modeling assumptions on long-term load prediction for offshore wind turbines, in: ASME 2009 28th International Conference on Ocean, Offshore and Arctic Engineering, American Society of Mechanical Engineers, 2009, pp. 1075–1083.
[30] Hermann Glauert, Airplane propellers, in: Aerodynamic Theory, Springer, 1935, pp. 169–360.
[31] Martin OL. Hansen, Helge Aagaard Madsen, Review paper on wind turbine aerodynamics, J. Fluid. Eng. 133 (11) (2011) 114001.
[32] Jakob Mann, Wind field simulation, Probabilist. Eng. Mech. 13 (4) (1998) 269–282.
[33] Annette Westerhellweg, et al., Wake measurements at alpha ventus-Dependency on stability and turbulence intensity 555, IOP Publishing., 2014, p. 012106. J. Phys. Conf.
[34] J.R. Morison, J.W. Johnson, S.A. Schaaf, et al., The force exerted by surface waves on piles, J. Petrol. Technol. 2 (5) (1950) 149–154.
[35] B. Mutlu Sumer, et al., in: Hydrodynamics Around Cylindrical Strucures, vol. 26, World scientific, 2006.
[36] C. Amzallag, et al., Standardization of the rainflow counting method for fatigue analysis, Int. J. Fatigue 16 (4) (1994) 287–293.
[37] Adam Nieslony, Determination of fragments of multiaxial service loading strongly influencing the fatigue of machine components, Mech. Syst. Signal Process. 23 (8) (2009) 2712–2721.
[38] Adam Nieslony, Rain flow counting method, set of functions with user guide for use with MATLAB, 2010. http://www.mathworks.com/matlabcentral/fileexchange/3026. Information on.
[39] Andrea Saltelli, et al., Sensitivity analysis practices: strategies for model-based inference, Reliab. Eng. Syst. Saf. 91 (2006) 1109–1125, 10-11.
[40] Gürkan Sin, Krist V. Gernaey, Anna Eliasson Lantz, Good modeling practice for PAT applications: propagation of input uncertainty and sensitivity analysis, Biotechnol. Progress 25 (4) (2009) 1043–1053.
[41] Nicholas Metropolis, Stanislaw Ulam, The Monte Carlo method, J. Am. Stat. Associat. 44 (247) (1949) 335–341.
[42] Gürkan Sin, et al., Global sensitivity analysis in wastewater treatment plant model applications: prioritizing sources of uncertainty, Water Res. 45 (2) (2011) 639–651.
[43] Francesca Campolongo, Andrea Saltelli, Sensitivity analysis of an environmental model: an application of different analysis methods, Reliab. Eng. Syst. Saf. 57 (1) (1997) 49–69.
[44] Francesca Campolongo, Jessica Cariboni, Andrea Saltelli, An effective screening design for sensitivity analysis of large models, Environ. Modell. Softw. 22 (10) (2007) 1509–1518.
[45] Sebastian Thöns, Michael H. Faber, Rücker Werner, Support structure reliability of offshore wind turbines utilizing an adaptive response surface method, in: 29th International Conference on Ocean, Offshore and Arctic Engineering, OMAE, 2010, 2010.
[46] Joint Committee on Structural Safety, *Probabilistic Model Code.* Joint Committee on Structural Safety, 2001. http://www.jcss.byg.dtu.dk.
[47] Det Norsk Veritas, Offshore concrete structures-DNV OS-C502, in: Det Norsk Veritas, 2012. Norway.
[48] Eurocode No, 2, Design of concrete structures, in: European Committee for Standardization, 1992.
[49] EN10029, Hot-rolled Steel Plates 3 Mm Thick or above - Tolerances on Dimensions and Shape, Danish Standards Foundation, 2010.
[50] AK DGGT, 1.4: Empfehlungen des Arbeitskreises „Baugrunddynamik “: Deutsche Gesellschaft für Geotechnik eV, in: V.(Hrsg.), 2002. Berlin 2012.
[51] International Electrotechnical Commission, et al., IEC 61400-3, in: Wind Turbines—Part 3: Design Requirements for Offshore Wind Turbines, 2009.
[52] Christina Koukoura, et al., Cross-wind fatigue analysis of a full scale offshore wind turbine in the case of windwave misalignment, Eng. Struct. 120 (2016) 147–157.
[53] Kolja Müller, Po Wen Cheng, Validation of uncertainty in IEC damage calculations based on measurements from alpha ventus, Energy Procedia 94 (2016) 133–145.
[54] Lisa Ziegler, et al., Design clustering of offshore wind turbines using probabilistic fatigue load estimation, Renew. Energy 91 (2016) 425–433.